ORIGINAL PAPER

A spectroscopic method to estimate the binding potency of amphiphile assemblies

D. R. Gauger · V. V. Andrushchenko · P. Bouř ·
W. Pohle

Abstract A fast and convenient spectroscopic methodology to determine the water uptake capacity of amphiphile assemblies studied in multilayer films is presented. This method was developed to provide a reliable but relatively simple tool for estimating the binding potency of such complex systems. The water-binding potency represents a general propensity of higher-order systems to bind or embed relevant ligands, such as various non-lipid effectors in the case of artificial lipid membranes. In this sense, the binding potency might contribute to a specific functional role of certain lipids. The essence of the new method is that the calibration of data measured by infrared (IR) spectroscopy against those directly obtained by Karl–Fischer titration (KFT) enables one to replace the expensive chemical–analytical technique by a more comfortable and efficient IR-spectroscopic protocol. This approach combines the easy handling, versatility, and availability of IR spectroscopy with the high accuracy of KFT. The usefulness of the procedure is demonstrated on an example set of six amphiphiles with a common chain length of 18 carbon atoms. Despite this similarity, the binding potency data differ tremendously in a way which can be correlated with the systematic variations introduced into the amphiphile structure. Going further beyond the methodical aspect, the scientific relevance of the data is comprehensively discussed especially in terms of the structural factors that govern the binding potency of amphiphiles. That is favored mainly by fluidity and disfavored mainly by inter-amphiphile binding networks. For phosphatidylcholine, our data are strongly in favor of a particular hydration model that involves primary water binding to phosphate as well as the formation of water semi-clathrates hosting the trimethylammonium moiety. Interestingly, stearylamine and diolein assemblies did not take up any water at all. This unexpected hydrophobicity is due to the unusual structures formed in these latter cases: rigid ammonium amide with a strong hydrogen-bonding/salt bridge network in stearylamine, and patches of inverted micelles in diolein, as revealed by molecular dynamics simulations.

Keywords Binding potency · Infrared spectroscopy · Karl–Fischer titration · Molecular dynamics · Amphiphiles (lipids, surfactants) · Hydration

D. R. Gauger · W. Pohle (✉)
Institute of Biochemistry and Biophysics,
Friedrich Schiller University of Jena,
Philosophenweg 12,
07743 Jena, Germany
e-mail: walter.pohle@uni-jena.de

V. V. Andrushchenko · P. Bouř
Institute of Organic Chemistry and Biochemistry,
Academy of Sciences,
Flemingovo nám. 2,
16610 Prague 6, Czech Republic

Introduction

Amphiphilic molecules are driven by the hydrophobic effect to assemble into higher-order structures which are held together by a number of weak interaction forces. This assembling process is important above all for the fields of molecular/cellular biology and technology/nanotechnology, and it concerns, respectively, two major groups of amphiphiles. The first group comprises lipids, representing the basic building blocks of biological

membranes and thereby accounting for the compartmentalization of the living matter. The second group is constituted by surfactants, which are involved in an increasingly huge number of practical applications. In nanotechnology for example, surfactants can serve as components or mediators in the construction of tailor-made nanostructures [1, 2].

An intriguing question addressed in cell biology is why so many structurally different lipids occur in nature [3]. Since it is hard to imagine that the barrier function of biomembranes alone would justify the existing wide range of lipid structures, the above question should be addressed to a more specific functionality connected with the manifold interaction and binding possibilities of lipids. However, the structural factors governing the interaction and binding potential of lipids are much less systematized than, e.g., those regulating the formation of different supramolecular structures, ranging from bilayers to non-lamellar phases [4-6]. While there is a shape concept [7] that explains the phase preferences in artificial lipid membranes satisfactorily in a first approximation, concepts predicting the interaction potential of such membranes from the lipid "primary" chemical structure are largely missed. Since the functions of biological membranes are realized mainly via non-lipid "effector" molecules anchoring in the bilayer (proteins are a prominent example), the ability or "capacity" of a given lipid species (or some mixture of them) to bind such "ligands" is an important inherent lipid property. A functional relevance of lipids, which is exerted via specific protein binding, was recently reported for, e.g., phosphatidylethanolamine (PE) and phosphatidylglycerol [3, 8].

The propensity of an amphiphile assembly (AA) to bind or retain a ligand is defined in the following as the "binding potency" (BP). It originates mainly in the attractive forces arising from the polar domain of an amphiphile and therefore depends on the ligand polarity. Apolar ligand molecules or molecular regions may be accommodated in the apolar domain of an amphiphile matrix mainly via van der Waals interactions, thus binding non-specifically with respect to the amphiphile primary structure. In Fig. 1, the term BP is defined more clearly. Above all, BP is a property attributed to a particular $(AA)_i$ and not to the underlying amphiphile "monomer", A_i. The sketch in Fig. 1 also illustrates the idea that BP may contribute to a specific functionality of a given A_i species, which could be helpful to rationalize the multitude of in vivo lipid structures.

Since BP depends mainly on the polar sites of an amphiphile, water is the logical probe for its quantification due to the following reasons: (a) water molecules are especially prone to hydrogen bonding by offering four potential binding sites (two donors and acceptors per
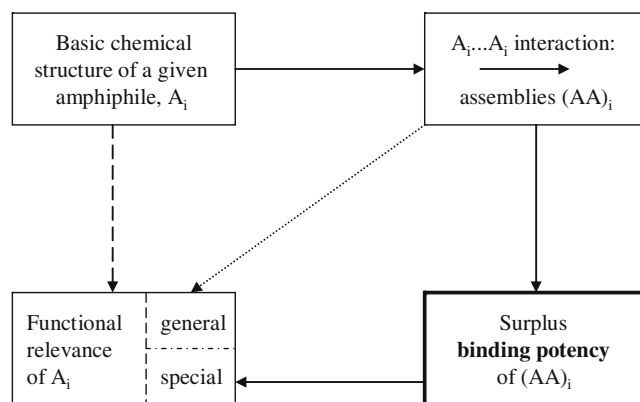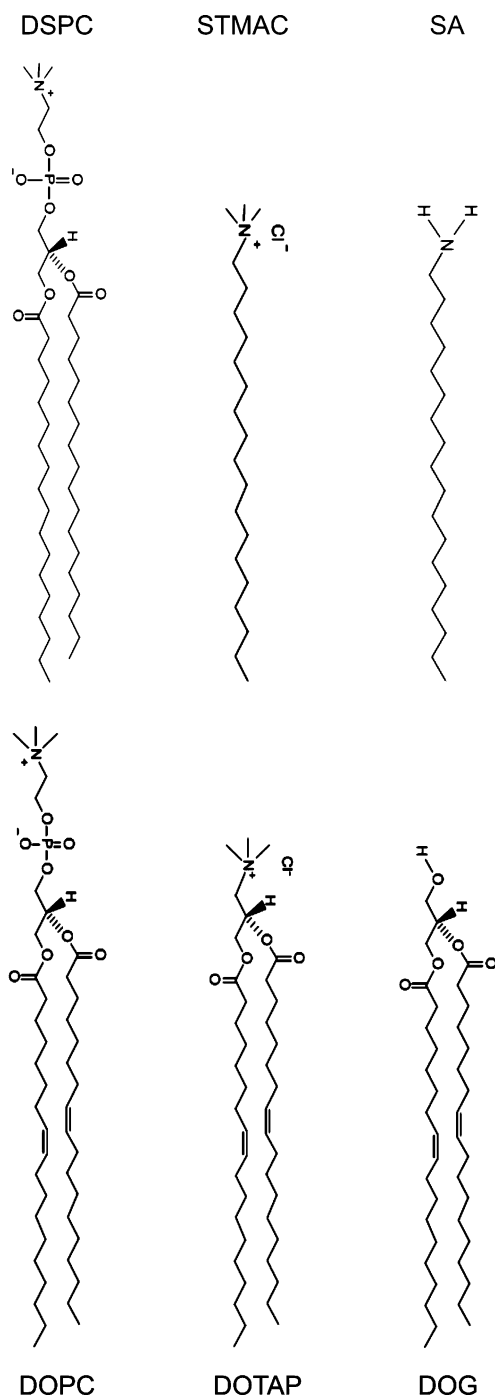

Fig. 1 Schematic sketch illustrating the definition of the binding potency in amphiphilic systems

molecule), (b) steric hindrance is minimized owing to its small molecular size, and (c), water is the main component of the "natural" medium of biomolecules in living systems. Hence, lipid hydration was well recognized as a topic of biological relevance [9] and has been reviewed regularly, e.g. in Refs. [9-13].

The aim of the present study was to develop a convenient practical method for exploring the BP of AAs by estimating their water-binding capacity. To that end, an IR-spectroscopic protocol which is based on a data set obtained by Karl–Fischer titrations performed with the same samples is proposed. IR spectroscopy is a well-proven powerful technique to study the structural implications of amphiphile assembling and aggregation from a submolecular up to the suprastructural scale [14-17], while KFT used in the present work for the calibration of the IR-spectroscopic data is the classical method to determine per se the water content in different materials down to trace amounts [18].

The set of amphiphiles chosen for this study and described in detail below (Fig. 2 and Table 1) comprises compounds of either biological or technological relevance. DSPC (for abbreviations see Table 1) and DOPC are abundant phospholipids [4], STMAC [19-21] and SA [22-24] are widely used surfactants, DOTAP is a prominent cationic lipid for gene transfer [25-27], and DOG is well known as a second messenger [28, 29], which stimulates protein kinase C [28-30] and promotes membrane fusion [31, 32].

It will be demonstrated below that the presented methodology is appropriate to provide a reliable quantitative measure for the BP of AAs. It is also applicable to other complex systems, for instance to polymers including biomolecules, such as nucleic acids, proteins or carbohydrates, or the higher-order structures or complexes formed by them. As to the AAs under study, some peculiar structural findings will be discussed in separate paragraphs

Fig. 2 Chemical structures of the six amphiphiles used in this study; see Table 1 for their full names

Materials and methods

Amphiphiles

In order to explore the potential of the experimental approach towards BP, a set of six different amphiphiles was investigated. These are listed in Table 1 and have one structural feature in common, namely the chain length of 18 carbon atoms (cf. Fig. 2). Taking DSPC as the origin of this series of compounds, two ways of structural variation were followed: chain unsaturation and the reduction of the polar domain in terms of size and charge. This has led to the two kinds of amphiphiles with saturated and unsaturated chains depicted in Fig. 2 in the top and bottom rows, respectively. Headgroup reduction was carried out in two steps: (a) withdrawal of the phosphate moiety leading to trimethylammonium (TMA^+) cations, and (b), removal of the charges (second and third columns in Fig. 2). Both these lines of structural modification of DSPC were completed in DOG having both unsaturated chains and an extremely small, uncharged headgroup ($-OH$).

The amphiphiles were purchased from the producers specified in Table 1. After confirming uniformity by thin-layer chromatography, the specimens were used without further purification.

Sample preparation and hydration

Films usually consisting of multilayers (that is, AA aggregates) were prepared by casting solutions of the amphiphiles in chloroform or methanol onto ZnSe windows (diameter 25 mm, thickness 2 mm; obtained from Vitron, Jena), as commonly used in IR spectroscopy, and unidirectionally stroking them by a plastic spatula until dryness. This procedure resulted mostly in homogeneous and well oriented samples with a mass of ca. 600 µg corresponding to an average thickness of about 400 monolayers. Unlike the other amphiphiles, DOG molecules did not readily orient and formed opaque deposits.

The films for the X-ray diffraction and KFT experiments were prepared on mica disks (diameter 10 mm, thickness 0.3 mm; from Jahre, Wilhelmshaven) and ZnSe windows, respectively, and differed from the usual IR samples by a higher mass.

Once the samples were free of solvent, their ZnSe supports were mounted into ad hoc constructed IR cells as displayed in Fig. 3 The cells were then sealed by appending little glass bulbs loaded with dry P_2O_5, different saturated salt solutions or pure water to produce a defined relative humidity (RH) between 0 and 100%. Before measurement, the samples were carefully equilibrated at least overnight. Hydration number, n_w, was taken as a measure of the water uptake and determined from spectroscopic data after

at the end of the paper. For diolein, molecular dynamics (MD) simulations, representing another useful tool to characterize amphiphile systems [33-36], were utilized to verify a starting hypothesis explaining the unexpected hydration behavior.

From the six compounds studied here, IR-spectroscopic hydration experiments have been carried out to date only for DSPC [37] and DOPC [38-41].

Table 1 List of the studied amphiphiles with the corresponding abbreviations and commercial sources

Amphiphile	Abbreviation	Source
1,2-Distearoylphosphatidylcholin	DSPC	Bachem[a]
Stearyltrimethylammonium chloride	STMAC	Fluka[b]
Stearylamine (octadecylamine)	SA	Sigma Co.[c]
1,2-Dioleoylphosphatidylcholin	DOPC	Sigma Co.
1,2-Dioleoyltrimethylammoniumpropane	DOTAP	Avanti polar lipids[d]
1,2-Dioleoylglycerol (diolein)	DOG	Sigma Co.

[a] Bachem, Heidelberg, Germany
[b] Fluka, Neu-Ulm, Germany
[c] Sigma Co., Munich, Germany
[d] Avanti Polar Lipids, Birmingham, USA

calibrating them with the results of coupled Karl–Fischer titrations (vide infra).

Methods

FTIR spectroscopy and X-ray diffraction

Spectra have been recorded by means of an IFS-66 spectrometer from Bruker (Karlsruhe) at ambient temperatures with a resolution of 2 cm^{-1} and a zero-filling factor of 2. For each spectrum, 32 scans were accumulated, and the apodization function of Hepp and Genzel was applied. Sample cell was measured against a reference cell (having the same RH, but no sample) using an automated shuttle device, which allowed for the compensation of any traces of water not bound to amphiphile. The OPUS software provided by Bruker was used for data processing. The water content of the films was estimated from the normalized absorbance, A_{wr}, derived from A_{OH}, the absorbance of the band near 3400 cm^{-1} emerging from the stretching vibrations of water, νOH, (cf. Fig. 4), by

$$A_{wr} = A_{OH}/A_{N}, \quad \text{where} \quad A_{OH} = A_{OHCH} - A_{CH}$$

and A_{N} is the absorbance of an IR band used for normalization.

Taking into account a large body of experiments, it turned out that most reproducible A_{wr} values were obtained from normalization by the absorbance of the νC=O band near 1740 cm^{-1} (see the DSPC spectrum in Fig. 7 below), arising from amphiphile carbonyl groups. Thus, $A_{N}=A_{CO}$ normalization was used. For STMAC and SA lacking the carbonyl groups, normalization had to be performed by A_{CH}, which represents the whole ensemble of νCH bands situated between 3050 and 2800 cm^{-1} (see Fig. 4, red part of the spectrum). Moreover, in the case of these single-chain amphiphiles a correction for the reduced number of methylene groups (roughly one half compared to the double-chain lipids) was done. All further spectroscopic details were described previously [37, 39, 40, 42].

X-ray diffraction (XRD) measurements in the small- and wide-angle ranges were carried out with synchrotron radiation utilizing the facilities of the DESY in Hamburg, especially the storage ring DORIS III and the X33 double-focusing monochromator-mirror camera of the EMBL. Cells as the one shown in Fig. 3 were used. The aim of these studies was to determine the phases adopted by the AAs under the conditions of our experiments. We have explained that XRD data are well suitable to complement IR-spectroscopic results and described the

Fig. 3 Photograph (**a**) and schematic drawing (**b**) of the infrared cells employed in the measurements; two ZnSe windows, one empty and one covered with the sample, were mounted by carefully screwing them together with all the other components. The sealed from the outer atmosphere metal or glass cylinder enclosing the cell windows was filled with water vapor of a defined relative humidity. Necessary RH was attained by placing different saturated salt solutions in the small glass bulbs, hermetically attached to the cylinder
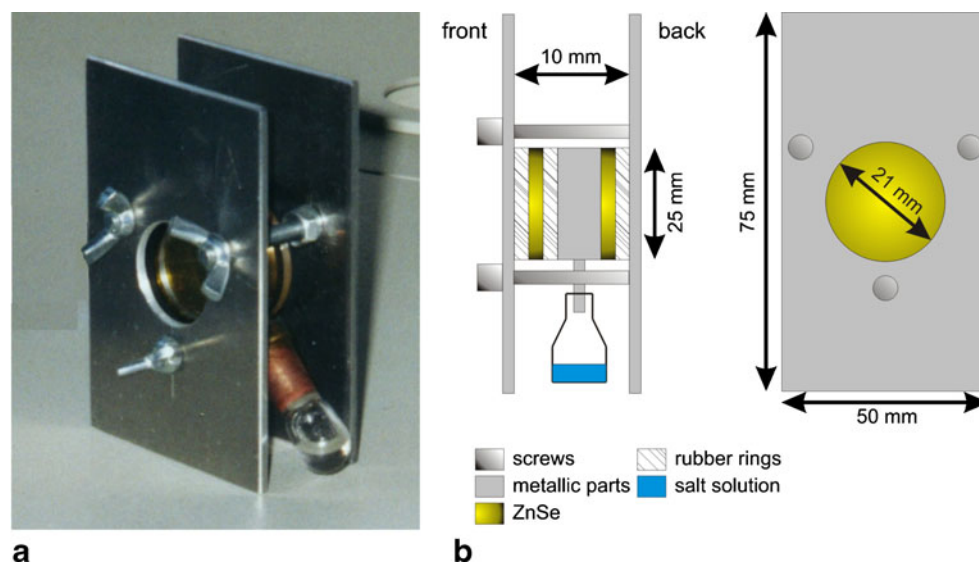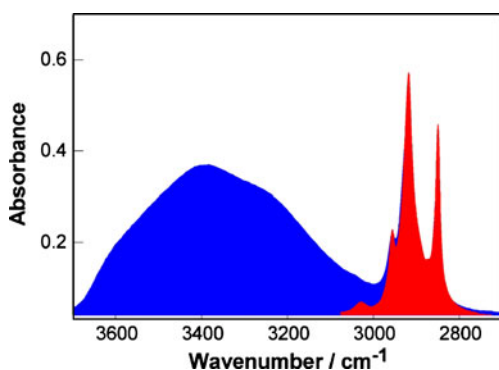
Fig. 4 IR spectrum of a typical hydrated amphiphile film showing the 3700–2700 cm^{-1} region essential for determining A_{wr}, the normalized absorbance of the νOH band of water; blue and red areas highlight the νOH absorption of the water adsorbed by the film and the ensemble of νCH bands arising from the amphiphile, respectively. The "red" profile could be obtained from water-depleted samples (at 0% RH) and used for subtracting A_{CH} from the overall A_{CHOH} values obtained at certain RH conditions (see text for details)

whole experimental procedure for XRD in detail recently [43].
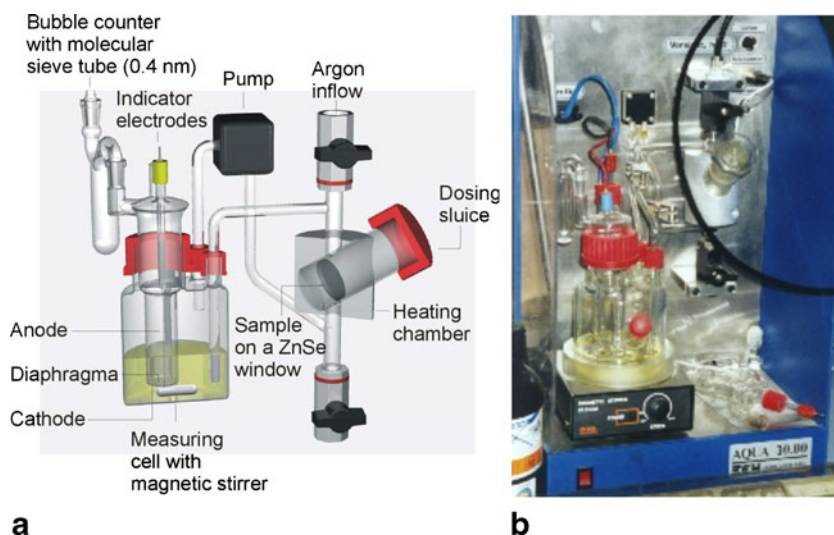
Karl–Fischer titration

A special variant of KFT [18] was applied in a number of cases to directly measure the exact hydration numbers resulting from the controlled water uptake (at defined RH) by the relevant AAs. These values can be used to calibrate the A_{wr} values obtained spectroscopically (as described above) for the same samples by correlating both data sets. This enables to eventually determine n_w directly from A_{wr} according to the calibration curve shown below in Fig. 6.

For the KFT measurements, the titrator Aqua 30.00 developed by ECH (Halle, Saale; the upgraded successor model Aqua 40.00 is described at www.ech.de) and based

on the principles of coulometry was employed. However, this device was ad hoc modified to meet the special sample demands required by IR spectroscopy. Related to the prototype presented in Refs. [44, 45], the dosing sluice had to be considerably enlarged such as to allow for the insertion of the amphiphile films together with their ZnSe supports. Figure 5 exhibits the whole apparatus in its modified version. The amount of water taken up by the AA films in preceding RH incubations at equilibrium could be reliably determined via the iodine which is used up in the Karl–Fischer reaction with water [18, 44].

Before titrating, each of the samples was warmed up to 110 °C in the heating chamber of Aqua 30.00 to desorb all the bound water. The water vapor was then pumped into the titration solution and detected by the indicator electrodes. More details on performing KFT in the Aqua 30.00 instrument are given in Ref. [45]. A combination of KFT and IR spectroscopy experiments was very shortly communicated in a "note and tip" elsewhere [46]. The overall function of n_w versus A_{wr} is linear only when A_{CO} is taken for normalization. In the case of normalization by A_{CH}, the curve is linear merely in the middle part (for n_w values between ca. 3 and 7), and adopts an exponential function outside of this region. Such a non-linearity may arise from the fact that the extinction coefficient of the νCH bands depends to some extent on the supramolecular structure of the AAs [14, 16]. By contrast, A_{CO} is rather insensitive to structural changes, including those which may occur during a hydration–dehydration cycle utilized in the experiments. Moreover, using A_{CO} for the normalization eliminates the need to correct for chain number and length necessary in the case of A_{CH} normalization. The comparability of the found n_w values (Table 2, below) is ensured no matter which normalization mode (with A_{CO} or A_{CH}) is used as the only relevant figure based on A_{CH} (for STMAC) was taken

Fig. 5 Karl–Fischer titrator Aqua 30.00 represented (**a**) by a schematic drawing and (**b**) a photograph of the instrument modified to meet the demands of the described methodology (see text for details)
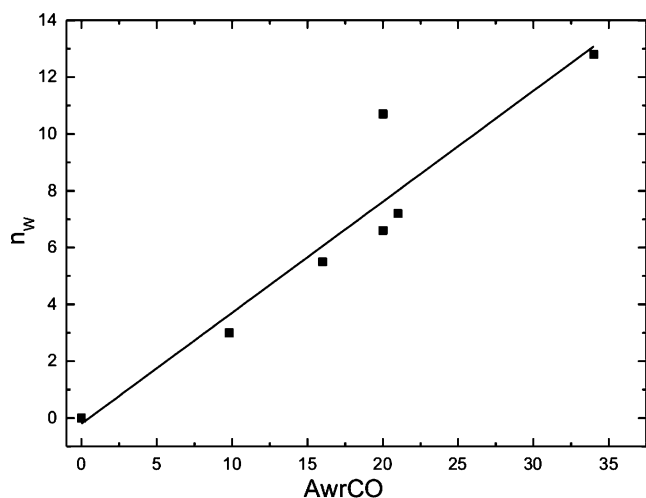
Fig. 6 Correlation of the hydration number n_w directly measured by Karl–Fischer titrations with the spectroscopically determined water absorbance A_{wrCO}; the latter is obtained by normalizing A_{OH} (absorbance of νOH band due to the amphiphile-bound water) with A_{CO} (absorbance of the νCO band of the amphiphile carbonyl groups). Slope and standard error for the straight line amount to 0.39 and 0.06, respectively

from the linear region of the n_w–A_{wrCH} function. Due to the updated relationship depicted in Fig. 6, the n_w/A_{wrCO} factor has to be slightly changed from the preliminary value of 0.34 given in [46] to 0.39.

Molecular dynamics

The MD simulations were done for DOG. An initial geometry of a single DOG molecule was created using MCM program [47]. All MD simulations were performed with the Amber 9 package [48] using supplied general amber force field (GAFF). Atomic charges for the DOG molecule were assigned semi-empirically with the help of the *antechamber* module from the Amber 9 package. Several systems consisting of either 6 or 60 DOG molecules were modeled. Such numbers of molecules were chosen to test the system behavior for distinctly different assembly sizes.

Generalized Born MD Six DOG molecules (DOG6) were put in several initial arrangements: random, bilayer and "genuine" micellar layouts (Fig. 11a,c,e, respectively, see below). The random structure was created with the aid of Packmol program [49], while the other two layouts were constructed using MCM program. Each of the DOG6 assemblies was subjected to 20 ns of generalized Born (GB) MD run. The implicit solvent was used to simulate the bulk DOG molecules around the six explicit ones by setting the dielectric constant $\varepsilon=2.0$ which is the value for carbohydrates supposed to approximately represent the bulk DOG molecules. The constructed DOG6 ensembles

were first subjected to 2500 steps of initial minimization with no cut-off. Then 20 ps equilibration was performed while heating the system from 0 to 300 K. The 20 ns production run was carried out at 300 K. Both equilibration and production steps were done with a 50 Å cut-off of Lennard–Jones interactions, using Langevin dynamics and employing the SHAKE algorithm on the H atoms with 2 fs time step.

Periodic boundary conditions MD Sixty DOG molecules (DOG60) were initially put in a bilayer arrangement with the help of MCM program (Fig. 12a, below). First an initial minimization with 2500 steps of steepest descent algorithm was done, followed by 3000 steps of conjugate gradient algorithm to relax possible bad geometrical contacts. Then the system was heated to 295 K within 20 ps. This was followed by 100 ps of equilibration at 295 K. Finally, the 20 ns production run was performed also at 295 K. The Lennard–Jones interactions were cut-off at 12 Å during the minimization and heating stages, while the cut-off of 10 Å was used for the equilibration and production stages of the simulation. Both equilibration and production were done using Langevin dynamics with the collision frequency $\gamma=1$ and employing SHAKE algorithm on the hydrogen atoms with a tolerance of 10^{-5} Å and 2 fs time step. The particle mesh Ewald method (PME) was used for handling long-range electrostatic interactions.

Periodic boundary conditions MD: system hydration The DOG60 structure obtained after 20 ns of MD simulations (Fig. 12b, which will be discussed in the "Hydrophobicity of diolein" section) was surrounded by a shell of 40 water molecules per lipid to model hydration in an excess of water (Fig. 12c). First, three stages of restrained initial minimization were done to relax possible bad geometrical contacts within the water shell and between the water and DOG molecules. Each stage consisted of 500 steps of minimization with steepest descent algorithm followed by 500 steps of minimization with conjugate gradient algorithm and the DOG atoms fixed with force constants of 80, 40, and 2 kcal/(mol Å^2) in each stage, respectively. Then unrestrained minimization was performed with 1000 steps of steepest descent and 1500 steps of conjugate gradient algorithms. Hereafter, the system was heated from 0 to 295 K within 20 ps keeping the DOG atoms fixed with a force constant of 10 kcal/ (mol Å^2). The heating was followed by 100 ps of equilibration at 295 K without any restraints. Finally, the 20 ns production run was performed at 295 K. All other parameters of the simulation were the same as described above for the periodic boundary conditions MD of DOG60.

Results and discussion

The water-binding potency for the six AAs under study is compared in the "Comparison of binding potency data" section. Some intriguing results, deserving more detailed insight, are discussed further in the sections "Hydrophobicity of stearylamine" and "Hydrophobicity of diolein".

Comparison of binding potency data

General aspects

Figure 7 displays survey IR spectra recorded for DSPC, STMAC, and SA. The top panel shows a comparison for water-depleted DSPC and STMAC. Main difference is the presence of the prominent bands due to C=O and PO_2^- stretching vibrations near 1740 and 1230/1085 cm^{-1}, respectively, only in DSPC. Upon hydration of STMAC, the broad bands due to the OH stretching and deformation vibrations of water emerge indicating some water uptake. This is not the case in SA (see bottom panel of Fig. 7). Another surprising feature of SA is the appearance of only one νNH band (due to stretching vibrations) instead of expected doublet. This will be further discussed below in the "Hydrophobicity of stearylamine" section.

The insets in Fig. 7 exhibit the expanded 1450–1600 cm^{-1} region of STMAC and SA spectra. SA is distinguished by a correlation-field splitting of both the CH$_2$ scissoring (see lower inset) and rocking (not shown) vibrational modes around 1470 and 720 cm^{-1}, respectively. This indicates a rigid and dense O$\perp$ chain packing mode (that is with othorhombic perpendicular subcells), which implies the presence of a lamellar crystalline phase in SA [50, 51]. By contrast, the lack of such a splitting in STMAC (cf. upper inset in Fig. 7) points at a lamellar gel phase with hexagonal chain packing [16].

The hydration numbers of the six studied AAs representing their BP at 98% RH which are listed in Table 2 turned out to be very different. Despite the structural similarity among the amphiphiles given by the equal chain length of 18 C atoms, the n_w values cover a wide range from 0 to about 11. Hydration numbers found in isopiestic adsorption measurements of films by gravimetry [12, 52] or IR spectroscopy are, as a rule, considerably smaller than those estimated by indirect (that is model-dependent) methods, such as XRD, differential scanning calorimetry or NMR spectroscopy [11, and references cited therein]. This difference is ascribed to the so-called water vapor paradox [52, 53], a phenomenon which was recently attributed to technical (instrumentation) implications [54].

The amphiphiles can be classified into three subgroups with high, medium, and zero BP distinguished by n_w values of about 11, 6, and 0, respectively. Generally, larger headgroup and the presence of charge(s) appear to favor an increased BP. For a better understanding of these BP differences, let us examine whether the studied AAs adopt solid (rigid) or fluid (liquid-crystalline) phases. It is widely accepted that fluid systems imbibe significantly more water than solid specimens, see, e.g., [11, 12]. The presence of double bonds and branches of the hydrocarbon chains as

Fig. 7 IR spectra of amphiphiles: hydrated and dry STMAC as well as dry DSPC are in the top panel, hydrated and dry SA in the bottom panel. The insets show selected regions of the spectra for hydrated STMAC (*above*) and SA (*below*) comprising δCH and δNH (only for SA) bands in expanded form
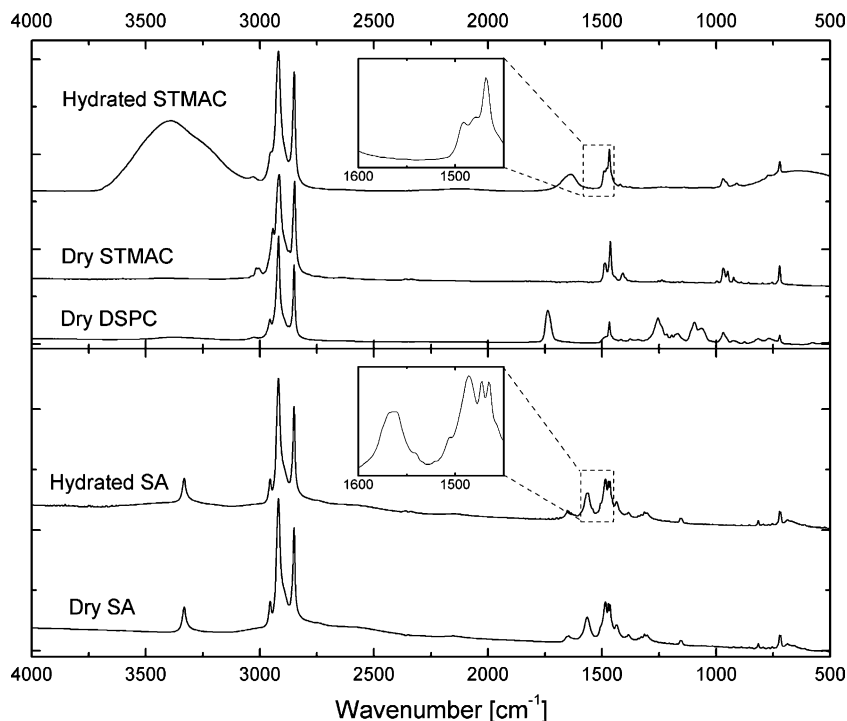
Table 2 Hydration numbers and wavenumbers of the symmetric C–H stretch of methylene groups for a set of amphiphiles with a common chain length of 18 C atoms; all values are averages of at least two measurements and were obtained at 98% RH

Amphiphile	SA	STMAC	DSPC	DOPC	DOTAP	DOG
n_w	0	4.5	6.3	10.7[a]	7.5	0
$\widetilde{\nu}_s CH_2 [cm^{-1}]$[b]	2850.5	2850	2851	2853.5	2854	2854.5
Phase	L_c	$L_{\beta'}$	$L_{\beta'}$	L_α	?	?, see text

The phases listed in the bottom line were determined by XRD experiments

[a] Value taken directly from Karl–Fischer titration experiments

[b] Values rounded to the next half unity

well as chain shortening make the amphiphiles indisputably more fluid [4]. The most common criterion to assess fluidity is certainly the transition temperature measured upon chain melting (T_t) transferring amphiphiles from solid (rigid) to fluid states (usually given by lamellar gel and liquid-crystalline phases). For example, the T_t values of 55 °C for DSPC and −17 °C for DOPC (these are averages of many respective data [4]), measured for lipid dispersions in excess water, demonstrate how huge the influence of chain unsaturation onto AA fluidity can be. Hence, DSPC, STMAC and SA with long, saturated chains and melting points above 50 °C [55] are solid, while all the unsaturated amphiphiles, DOPC, DOG (with a melting point of 2 °C [56]) and DOTAP, are fluid.

Reliable information about amphiphile fluidity is also provided by IR spectroscopy, and can be conveniently obtained in our experiments simultaneously with the quantitative hydration data. As empirically established, the wavenumbers of the νCH bands arising from methylene groups, $\widetilde{\nu}CH_2$, increase significantly with amphiphile fluidity [14, 16, 39, 40]. In particular, these wavenumbers undergo an abrupt upshift by about 2–2.5 cm^{-1} upon chain

melting in both the thermotropic [14, 16] and the lyotropic case [39, 40]. The wavenumbers for the band due to symmetric methylene νCH mode, $\widetilde{\nu}_s CH_2$, are listed in Table 2. Since the borderline between solid and fluid phases taken at the midpoints of the $\widetilde{\nu}_s CH_2$-T and $\widetilde{\nu}_s CH_2$-n_w curves is at about 2852 cm^{-1} [14, 16, 39, 40], the rough solid–fluid classification made for the six amphiphiles used in this study by the T_t values and melting points holds true for the film samples, too (cf. Table 2). Moreover, these assignments are corroborated by the results of concomitant XRD studies revealing that DSPC and STMAC form lamellar gel (L_β) phases, while SA adopts a lamellar crystalline (L_c) phase. Exemplarily for the XRD studies, Fig. 8 displays data for hydrated DSPC films. These show unambiguously the signature of a gel phase with tilted chains, called $L_{\beta'}$, in particular by the pattern of reflexes in the wide-angle region with the main peak and a shoulder towards higher reciprocal spacings [57, 58]. The long and short spacings of 6.7 and 0.42 nm found for our films are exactly the same as reported previously for DSPC dispersions (cf. Refs. [59] and [58], respectively). Both these solid phases, L_β and L_c, could be mainly distinguished by

Fig. 8 Results of X-ray diffraction performed for a hydrated DSPC film (equilibrated for 3 days at 100% RH) in the small- (SAXS, left) and wide-angle X-ray scattering ranges (WAXS, right); the SAXS peaks are equidistant thus revealing a lamellar phase which has a periodicity of ca. 6.7 nm. The WAXS pattern with main peak and shoulder is typical for the $L_{\beta'}$ phase (see text). The maximum of the main peak corresponds to an inter-chain spacing of ca. 0.42 nm
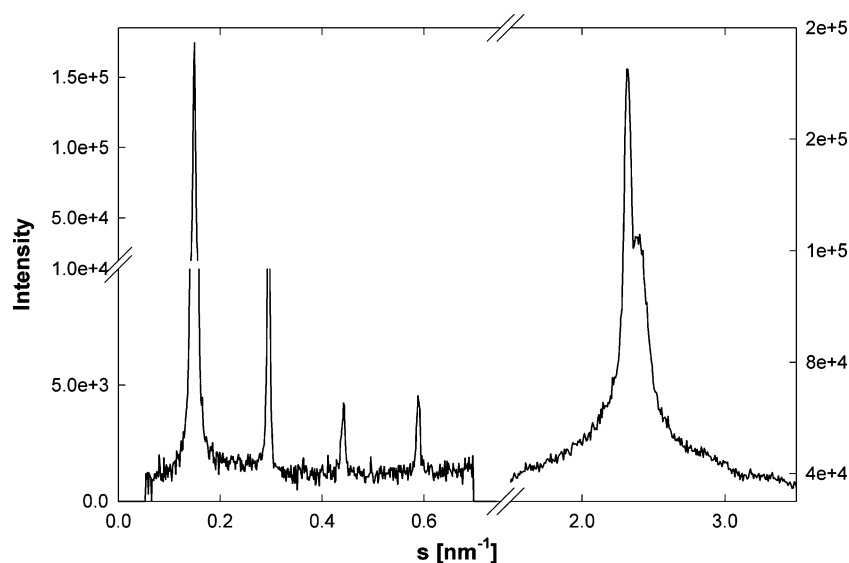
the XRD reflexes in the wide-angle range and by the correlation-field splitting of the δCH_2 modes, which is typical for crystalline phases [50, 51]. Such a splitting was observed only for SA (Fig. 7, lower inset).

To summarize these results, the AAs in the upper and lower rows of Fig. 2 represent solid and fluid systems, respectively. The water adsorption isotherms measured spectroscopically for all these amphiphiles are shown in Fig. 9 in panels a and b, respectively.

Solid-state amphiphile assemblies and the possibility of water chlathrate formation

The adsorption isotherm of SA in Fig. 9a illustrates that there is no measurable water uptake under our experimental conditions, as mentioned before. The AAs of STMAC and DSPC imbibe water, not only in different amounts, but also in a different way as indicated by the various shapes of the curves. According to the classification of adsorption isotherms into five types [60], DSPC and STMAC belong to types II and III revealing them as 'strong' and 'weak' water binders [12, 52, 60], respectively. Consistently, DSPC adsorbs more water than STMAC as can be seen from the n_w values, which are by 1.5–2 units higher for DSPC throughout almost the whole RH range (Fig. 9a). This n_w difference originates in a significant initial water binding by DSPC at RH<25%, typical for PC [12, 39, 40, 61], and not observable for STMAC. The approximately two surplus water molecules bound to DSPC can be easily ascribed to the presence of the phosphate group. The PO_2^- moiety is regarded as the primary water-binding site in phospholipids as well as in other biomolecules [62–64], and references cited therein]. A BP of the PO_2^- moiety of about two water
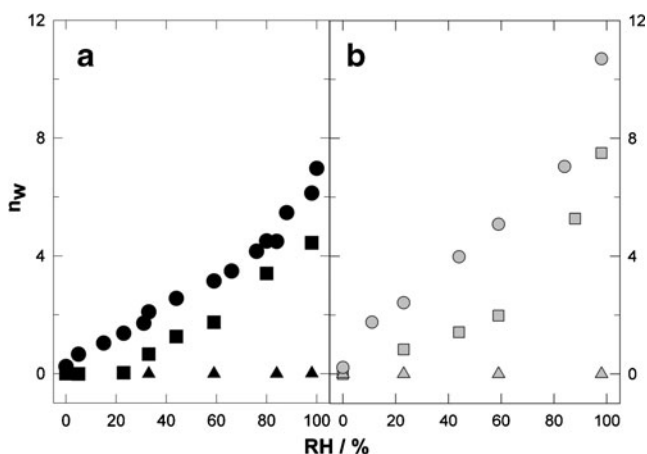
Fig. 9 Adsorption isotherms obtained for the solid and fluid amphiphiles under study and displayed in the *left* (**a**) and *right panels* (**b**) with *black and gray symbols*, respectively: triangles are for SA and DOG, squares for STMAC and DOTAP, and circles for DSPC and DOPC, respectively; the isotherms were constructed from IR-spectroscopic data. DOPC values were taken from Ref. [64]

molecules was also reported previously for phospholipids [12, 52, 63, 65, 66] and for methylphosphocholine (MePC), studied as a phospholipid model [67]. Consequently, the major part of the hydration water molecules must be bound to (an)other site(s) most likely related to the positively charged trimethylammonium (TMA$^+$) moiety. From the background of literature data given in the following, clathrate-like water clusters located around TMA$^+$ probably as semi-clathrates can be suggested for STMAC and DSPC. Water clustering was found for various hydrophobic molecules, e.g., as clathrate hydrates in the cases of alkylamines and quaternary ammonium salts [68]. The details of the hydrogen bonding in clathrates are not well known [69], but often the functional group (for instance –NH$_2$ in alkylamines) is hydrogen bonded to the water lattice [69]. The anions of quaternary ammonium salts are likewise involved in the water network surrounding the cation [70]. A preferred hydration number in clathrates or chlathrate-like structures is five [68, 71, and references cited therein], often realized in rings [66, 68, 71]. Clathrate hydrate formation was also reported for choline [72], and suggested for phosphatidylcholine (PC), in contrast to their PE counterparts [33, 34] and MePC [67] from the results of molecular dynamics simulations. The hydration model with approximately two waters bound to PO_2^- and five waters anchored around TMA$^+$, presented here for DSPC and STMAC, is in a very good agreement with the hydration picture proposed for solid dimyristoyl-PC (DMPC) [66]. The latter model was deduced from studies with a different methodology (NMR spectroscopy at sub-zero temperatures) and involves also a five-member ring situated around the TMA$^+$ moiety [66]. A further experimental evidence for "clathrate-like water structures near the hydrophobic choline group" was very recently obtained by ultrafast polarization selective vibrational pump-probe spectroscopy applied to aligned multibilayers of dilauroyl-PC (DLPC) [73]. In accord with the conclusions drawn for solid DMPC [66] and DSPC (this study), two major types of water are proposed to exist in DLPC films, comprising phosphate- and choline-associated water species with pertinent n_w values of 1–4 and 1–12, respectively [73].

Fluid-state amphiphile assemblies and further aspects of water chlathrate formation

The adsorption isotherms of the three fluid amphiphiles depicted in Fig. 9b are qualitatively very similar to those of their solid counterparts in each case. While DOG surprisingly did not take up any water at all, DOTAP and DOPC imbibe water, and even considerably more than their solid analogs, STMAC and DSPC. The shapes of the DOTAP and DOPC isotherms again reveal them to belong to types II and III, as STMAC and DSPC, respectively. However,

the fraction of water initially bound to DOPC is about 2.5 molecules at 25% RH, which is by ca. 1 water/lipid higher compared to DSPC. The surplus n_w increment of 2.5–3 found for DOPC versus DOTAP throughout the whole range of n_w values (Fig. 9b) is accordingly larger than for the DSPC-STMAC pair (1.5–2 units). Presumably, the n_w surplus of DOPC vs. DOTAP can be again attributed to the presence of the phosphate group in DOPC which seems to bind about one water molecule more than in the solid counterpart, DSPC.

Comparing the two PCs, a BP increase from DSPC to DOPC by about 4.5 water molecules per lipid is noticed (Table 2). This can be unambiguously attributed to the higher fluidity of DOPC adopting a liquid-crystalline phase evidenced by both the higher $\tilde{v}_s CH_2$ value and the XRD results. The latter reveal the L_α phase to exist in highly hydrated DOPC films, while DSPC maintains a gel phase under the same conditions (Fig. 8, Table 2). Due to the larger cross-section area of oleoyl chains (related to stearoyl), originating from the *cis*-configuration at the double bond in the C9 position, the headgroup region of DOPC provides potentially more space for accommodating bound water molecules than that of DSPC. The fluidity-caused increase of BP found when going from DSPC to DOPC is overall (see Fig. 9) and, thus, appears to hold also for the phosphate group which is obviously able to bind about one surplus water molecule in the latter case.

Gravimetrically measured adsorption isotherms [52] strongly resemble those which we obtained spectroscopically, and the hydration numbers determined at RH=98% of about 13 for DOPC and 8 for DOTAP [52] are very similar to the values given in Table 2. A good agreement between gravimetric and spectroscopic isotherms was also found for lipids with phytanoyl chains [61].

Apparently, the polar domains of the fluid amphiphiles DOPC and DOTAP can provide interstitial space sufficient (or have a "binding capacity" as big as) to allow for the formation of water clusters with seven to eight water molecules. On the contrary, the AAs of DSPC and STMAC adopting the gel phase can accommodate the five-member ring clusters of water [66] at most.

Presumably, the clathrate-like water structures anchor at the amphiphile headgroups [69], but the detailed nature of the sites directly involved in this binding is not clear. The putative presence of such water clusters also in the phosphate-depleted amphiphiles STMAC and DOTAP suggests the TMA$^+$ moiety to be included in the water binding, the more so as quaternary amines are well known to accommodate water clathrates [68]. A docking of one or more water molecules to TMA$^+$ could be realized, for example, via (methyl-)C–H···O hydrogen bonds. Due to the influence of the adjacent positively charged (electron-deficient) nitrogen, methyl hydrogens are considerably

acidified thus enabling the formation of relatively strong C–H···O hydrogen bonds. Hence, while in phospholipids the phosphate oxygens may be the first choice to anchor the water clusters (which, e.g., could be bridged by directly H-bonded water molecules), the TMA$^+$ moiety can be involved for that as well.

The unexpected zero BP in SA and DOG deserves also a thorough consideration. At first glance, SA can be suspected to be more prone to water binding than STMAC since the polar amino groups of SA should be a more potent H-bonding donor site than the C–H groups present in the headgroup region of STMAC. Moreover, although both these surfactants appear to be compatible with the formation of water clathrates [68, 69], the latter occurs only in STMAC (with a BP of nearly 5, see Table 2) and is evidently impossible in SA. This will be further discussed in the "Hydrophobicity of stearylamine" section.

Taking into account the extremely high fluidity of DOG revealed by the spectroscopic data (Table 2), the zero BP found for the DOG assemblies is even more intriguing than in the case of SA and will be regarded separately in the "Hydrophobicity of diolein" section.

Hydrophobicity of stearylamine

The surprising zero BP of SA films will be considered in context with another curious result, namely the seemingly irregular appearance of only one νNH band situated at 3332 cm^{-1} (Fig. 7). The latter finding contradicts one of the cornerstones of the IR spectroscopy of primary amines that implies the obligatory emergence of two νNH bands due to the antisymmetric and symmetric modes [74-79]. This conflicting situation has encouraged us to comprehensively reconsider the IR spectra of primary aliphatic amines reported so far. As briefly described in a short note [80], this search of the relevant literature including textbooks [74-79], catalogues [81-83], and recent original papers [22, 24, 84] revealed the existence of essentially two types of amine spectra. Type I comprises the canonical spectra with two νNH bands described in any of the numerous textbooks devoted to IR spectroscopy [74-78] or organic chemistry [79] as exclusively representing primary amines. Interestingly, such spectra arise only when the amines are in a fluid state [82, 83] or in solution [85]. On the other hand, type-II spectra with a single νNH band, like the one reported here for SA, emerge whenever the amines are in a solid state [22, 24, 81, 83]. Therefore, these type-II spectra were already widely documented, but an adequate interpretation has never been attempted to the best of our knowledge. Figure 10 exemplarily shows the IR spectra of dodecylamine (DA) taken from Ref. [83] in the fluid (melted film) and solid (smeared film) state, representing
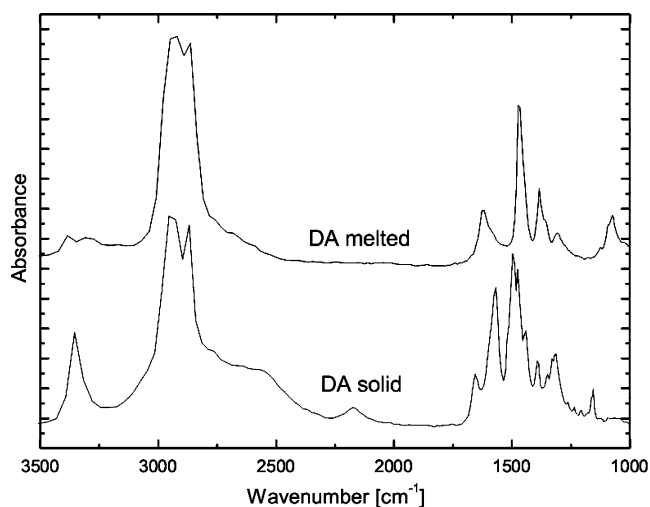
Fig. 10 Representative IR spectra for fluid (*above*) and solid (*below*) dodecylamine (DA) taken from the catalogue of NIST [83] with permission

type-I and -II spectra, respectively, for one and the same compound.

A further striking feature of the type-II spectra is the spectroscopic signature of ammonium. This is indicated by both the broad stretching vibration (νNH_3^+) band near 2900 cm^{-1} (superimposed by the νCH_2 and νCH_3 bands) shown in Figs. 7 and 10 and the doublet arising from the antisymmetric and symmetric deformation (scissoring vibration) modes (δNH_3^+) at 1568 and 1486 cm^{-1}, respectively (cf. Fig. 7, bottom inset). Even more spectral differences can be seen in Fig. 10 and were detailed in Ref. [80]. All these observations lead to the conclusion that it is not a primary amine, RNH_2, but rather the corresponding ammonium amide, $RH_2N^+H\cdots N-HR$, that gives rise to the type-II spectra (with $R=C_{18}H_{37}$ in the case of SA) [80].

This interpretation implies that a self-dissociation reaction involving a proton transfer from one amino group to the other has to proceed. The principal driving force for the proton transfer may arise from the strong attractive forces existing as a consequence of the tight N^+–$H\cdots N-$ hydrogen-bonding/salt bridge network formed in the polar region of solid fatty amines. Presumably, the interactions inside the N^+–$H\cdots N-$ network are energetically favored in comparison to the H bonds that could be formed between the neutral amino groups of the "nominal" primary amines. The resulting ammonium amide structure is additionally stabilized by the close chain packing in these specimens. The observed inability of SA films to bind measurable amounts of water from the gas phase might be a result of such strong hydrogen-bonding/salt bridge networks preventing any penetration (and binding) of water to the amphiphile headgroups including the formation of water clathrates.

Similar intermolecular networks were described previously for other systems. In PE, e.g., they involve the PO_2^- and NH_3^+ moieties [86-89], and they are supposed to account for the remarkable decrease of water binding found for PE in comparison to PC [11, 38, 52, 64, 88, 89]. The IR-spectroscopic evidence of such networks was described for PE in water dispersions [90] and in films [38]. In the latter case, an almost complete water refusal by the headgroups of saturated PE was found and theoretically rationalized [38]. Another example of a strong water-repelling network formed, however, exclusively by salt bridges, was reported for 1,2-dimyristoyltrimethylammoniumpropane chloride (DMTAP) [91], an analogue of DOTAP. In such particular cases of strong intermolecular interactions as in ammonium amide and DMTAP, the existence of charges is no longer favorable in terms of BP, as it was observed sometimes elsewhere and mentioned above ("General aspects" section).

The presence of ammonium amides in solid fatty amines as deduced here for SA films sheds a new light on this class of compounds, especially in terms of their broad practical application as surfactants.

Hydrophobicity of diolein

The zero BP of DOG is particularly astonishing because of its high fluidity. Note that the other two AAs with oleoyl chains and a similar fluidity as DOG, namely DOPC and DOTAP, show the highest BP values of all studied AAs (Table 2). A very sensitive radioactive technique revealed a very weak water binding to DOG up to n_w of 0.03 [92], which is too low to be detected by IR spectroscopy.

A similarly strong hydrogen-bonding network as that accounting for the zero BP in SA is not present in DOG, since its broad νOH band is located at fairly high wavenumbers near 3490 cm^{-1} (data not shown) indicating rather weak hydrogen bonds in this AA system. In fact, the H bonds in DOG must be even weaker than those formed in bulk water with OH values around 3400 cm^{-1}.

An alternative approach for explaining the DOG hydrophobicity is to assume a peculiar assembling mode that renders the potential water-binding sites sterically non-accessible. Previous investigations using spectroscopic resonance methods have provided evidence that DOG could form micelle-like assemblies. From the results of ESR spin-label studies, the formation of isotropic dispersions of non-hydrated "oil droplets" was proposed for 1,2-dimyristoylglycerol (DMG) [93, 94]. Similar dispersions can be also suggested for neat DOG which is very similar to DMG. Furthermore, adding DOG to PC resulted in the emergence of an isotropic component in the ^{31}P-NMR spectrum [95] which was tentatively ascribed—as one of the possible explanations given in Ref. [95]—to

Fig. 11 Starting structures for the MD simulations of DOG6 assembly (*top*): random initial arrangement (**a**), bilayer initial arrangement (**c**) and "genuine" micellar initial arrangement (**e**), and the snapshots (*bottom*, **b**, **d** and **f**) obtained after 20 ns of Generalized Born MD simulations
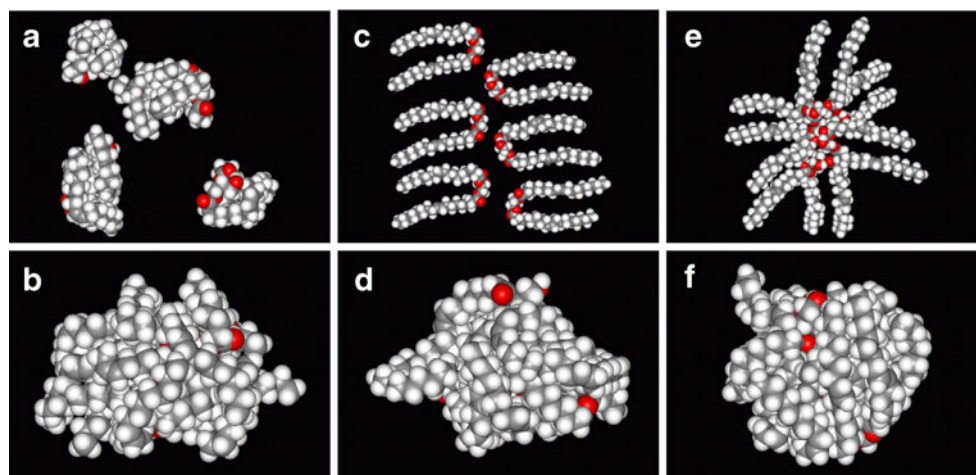
"DOG micelles sandwiched between the leaflets of PC bilayers".

Since the opaque DOG films obtained under our standard preparation conditions did not provide any usable X-ray reflexes, we have searched for energetically favorable higher-order structures by means of molecular dynamics. Unfortunately, there is no information (or substantiated idea) about the size of the DOG assemblies formed under our experimental conditions. Hence, the MD simulations were performed for two extremely different cases with systems comprising 6 and 60 amphiphile molecules. The initial structures and the MD results are shown in Figs. 11 and 12. and reveal that all the systems collapsed spontaneously into a globular micelle-like sphere regardless of system size (6 or 60 DOG molecules), initial configuration

(random, bilayer, or micellar), and solvent model (implicit or explicit). In each case, the structural transition occurs within the first few nanoseconds, and the globular structure is maintained throughout the simulations as shown by stable rms deviation profiles (not shown). This behavior is in striking contrast to that of hydrated PCs which consistently adopt (or maintain) bilayer structures in the course of MD simulations [33, 96, 97].

The snapshots taken upon the stabilization of the systems (Figs. 11b,d,f and 12b) reveal that the DOG globules are of the inverse micellar type. Such an arrangement is expected when considering the ratio of the cross-section areas due to the (extremely small) polar and (large) apolar domains. As a consequence, the polar hydroxyl and carbonyl groups are mostly hidden inside

Fig. 12 Starting structures (*top*) for the MD simulations of DOG60 assemblies: neat DOG60 system (**a**) and fully hydrated (by adding 40 water molecules per amphiphile) DOG60-water system (**c**); pictures **b** and **d** (*bottom*) represent the snapshots after 5 ns of periodic boundary conditions (PBC) MD simulations. The resulting structure of the neat DOG60 simulation (**b**) was used as an input structure to construct the hydrated system (**c**) as detailed in the "Molecular dynamics" section
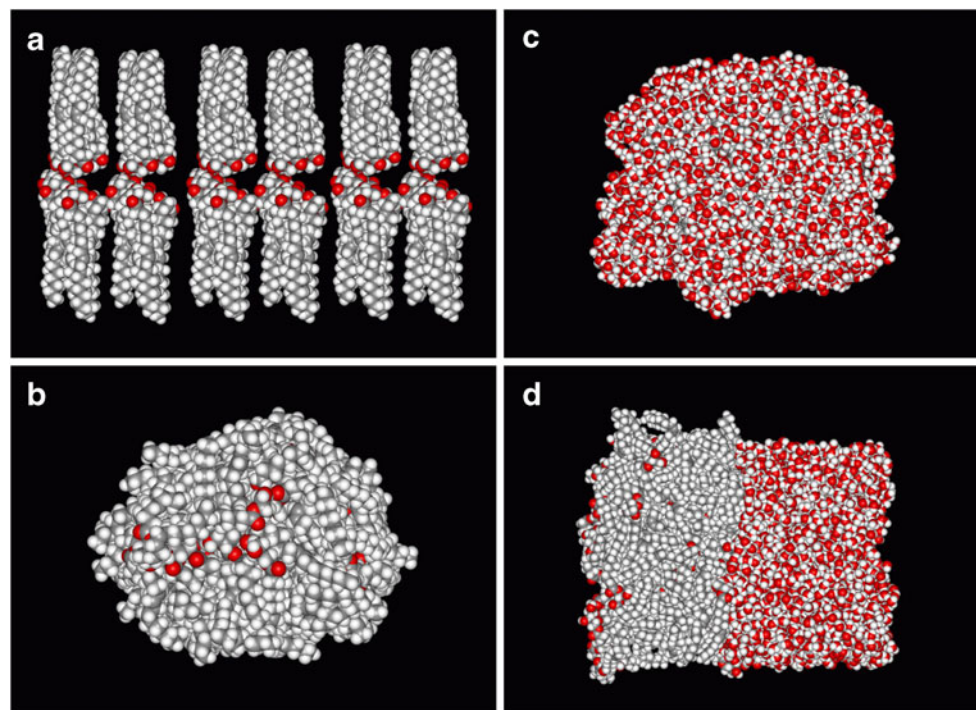
Fig. 13 Snapshots of six unit cells of the PBC simulations of neat DOG60 system taken at different times: **a** 0 ns; **b** 5 ns; **c** 7 ns; **d** 20 ns
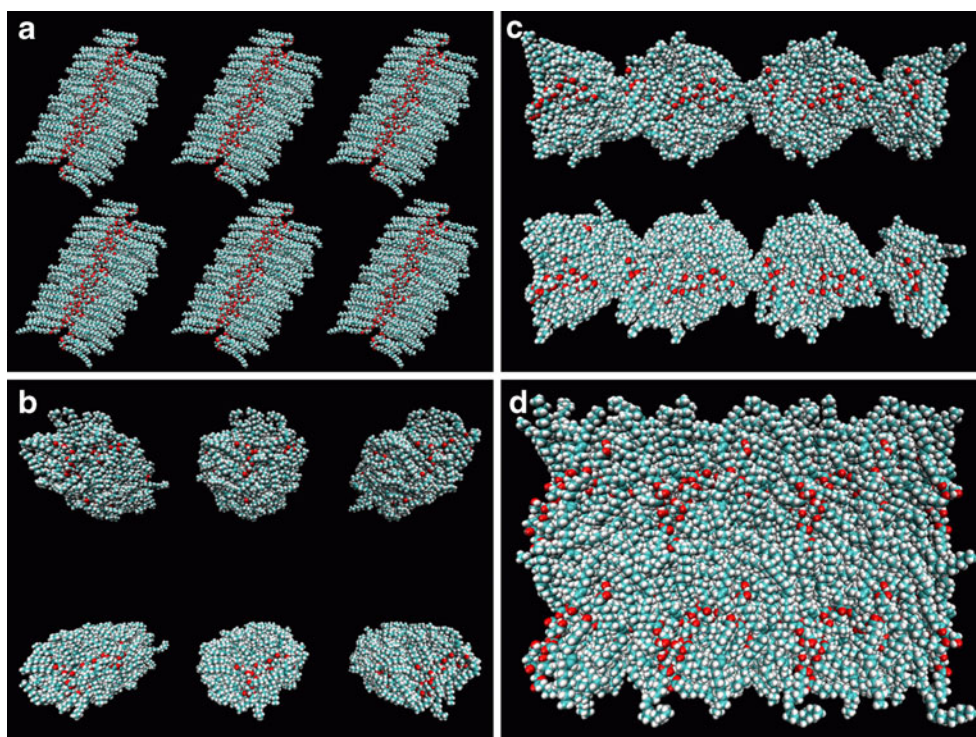
the inverse micelles and, hence, cannot act as water-binding sites (Figs. 11 and 12).

Interestingly, the reversed micellar arrangement of DOG prevents water molecules from penetration inside the globules even in large water excess. MD simulations of "strongly hydrated" DOG60 (n_w=40) reveal a clear separation of the water from the DOG phase occurring already after a few nanoseconds (Fig. 12c,d). This simulated behavior fully agrees with the experimentally found zero BP of DOG films. It should be mentioned that a zero BP obviously can be achieved only if the inner polar domain is sealed "round about" by a closed hull of apolar chains, such as shown in Figs. 11b,d,f and 12b, since nonlamellar phases with "open ends", like inverse ribbon (P_α) or hexagonal (H_{II}) phases, do imbibe small but significant amounts of water [42, 98, 99]. In other words, the found hydrophobicity likewise excludes the presence of noticeable fractions of ribbon or H_{II} phases in our DOG samples.

Rather, the micelle-like globules formed therein can be supposed to aggregate into irregular patches, as shown in Fig. 13, which eventually coalesce to opaque specimens. This explains not only the zero BP of DOG, but also the unusual tenacity observed during film preparation and the non-appearance of any X-ray reflexes. Altogether, the MD results presented here provide the first direct evidence of micelle formation in DOG assemblies, besides rationalizing their water-repelling behavior.

Conclusions

A new experimental methodology for quantifying the binding potency of amphiphile assemblies is described. BP is considered an important factor contributing to a specific functional role of membrane lipids and, thus, to a better understanding of the large diversity of lipid structures occurring in the living world. BP is also of great interest for surfactants due to their enormous practical application in various technological fields.

The method utilizes water for probing the BP of AAs and combines the convenient handling of infrared spectroscopy with the high accuracy of Karl–Fischer titration. Here, it was successfully employed to characterize an example set of six different amphiphiles with a common chain length of 18 C atoms, but also with ad hoc designed gradual structural variations. This set of compounds comprises three solid and three fluid amphiphiles with saturated and unsaturated hydrocarbon chains, respectively. The polar domain was reduced stepwise in size and charge in both cases.

The water BP measured at 98% of relative humidity differs for the studied AAs in a wide range of hydration numbers between 0 and 11. These differences can be explained by the specific properties of the assemblies which in turn are governed by structural features of the amphiphile monomers.

There is a variety of factors promoting or restricting the BP of AAs. On the one hand, amphiphile fluidity, which is largely determined by the chain structure, as well as

increased headgroup size and charge generally favor BP. On the other hand, BP also depends strongly on the availability and steric accessibility of the potential binding sites. As revealed by our data, BP can be significantly reduced, or even become zero, if the binding sites are either involved in strong inter- or intramolecular networks formed by hydrogen bonds and/or salt bridges or hidden inside of nonlamellar assemblies. Thus, the BP of AAs is not straightforwardly predictable from the amphiphile monomer structure.

In phosphatidylcholine, which represents the most abundant class of phospholipids, the outstanding role of the phosphate group as a primary water-binding site is clearly demonstrated. However, the larger part of hydration water is most probably arranged as clusters, e.g., as semi-clathrates around the trimethylammonium moiety. These water clathrates are bound much more weakly than the water attached at phosphate. One may speculate about a possible role of these loosely anchored water clathrates. Presumably, they could act as some kind of a placeholder filling the voids inherently present in the polar domain of PC. On demand, these clusters could be easily replaced by some functionally important "effector" ligand or a relevant part of that.

A striking exception from the rule that fluidity promotes binding is the zero BP found for diolein. This is caused by an unusual mode of assembling revealed by the results of MD simulations. Hence, DOG molecules assemble spontaneously into globular super-structures resembling inverse micelles. Their potential binding sites (–OH and >C=O) are mostly hidden inside the micelles and thus become inaccessible for water binding.

Another unexpected finding is the zero BP for stearylamine. The spectroscopic data indicate that the hydrophobicity of SA arises from a strong hydrogen-bonding/salt bridge network which is a crucial part of the ammonium amide arrays formed as the consequence of a self-dissociation reaction proceeding in the nominal primary amine. The tightness of this network is a major factor to expel water from the potential binding sites in SA. A comprehensive literature search devoted to the IR spectra of primary amines has led to the conclusion that the ammonium amide formation appears to be a general feature of fatty amines whenever these are in a solid state.

The described structural implications of the AAs under study can be important in two more far-reaching respects: for the practical applications of fatty amines as surfactants in technology and nanotechnology, and in terms of biological relevance. The latter may concern the functional role of DOG in cellular biology, and, as a novel aspect, the water clathrates in PC.

References

1. Texter J (2007) Structure of surfactant and amphiphile assemblies. Taylor & Francis, New York
2. Tadros TF (2006) Applied surfactants: principles and applications. Wiley VCH, Weinheim
3. Dowhan W (1997) Ann Rev Biochem 66:199–232
4. Marsh D (1990) CRC handbook of lipid bilayers. CRC, Boca Raton
5. Koynova R, Caffrey M (1994) Chem Phys Lipids 69:1–34
6. Koynova R, Caffrey M (1998) Biochim Biophys Acta Rev Biomembranes 1376:91–145
7. Israelachvili JN, Marcelja S, Horn RG (1980) Quart Rev Biophys 13:121–200
8. Kim K, Ahn T, Yun CH (2003) Biochemistry 42:15377–15387
9. Rand PR, Parsegian VA (1997) In: Epand RM (ed) Lipid polymorphism and membrane properties, current topics in membranes 44. Academic, San Diego
10. Hauser H (1975) In: Franks F (ed) Water—a comprehensive treatise. Plenum, New York
11. McIntosh TJ, Magid AD (1993) In: Cevc G (ed) Phospholipids handbook. Marcel Dekker, New York
12. Jendrasiak L (1996) J Nutr Biochem 7:599–609
13. Milhaud J (2004) Biochim Biophys Acta 1663:19–51
14. Casal HL, Mantsch HH (1984) Biochim Biophys Acta 779:381–402
15. Scheuing DR (1991) Fourier transform infrared spectroscopy in colloid and interface science. American Chemical Society, Washington
16. Lewis RNAH, McElhaney RN (1996) In: Mantsch HH, Chapman D (eds) Infrared spectroscopy of biomolecules. Wiley-Liss, New York
17. Special volume 96 of Chem Phys Lip (1998) Infrared spectroscopy of membrane lipids
18. Scholz E (1984) Karl Fischer titration. Springer, Berlin
19. Scarzello M, Klijn JE, Wagenaar A, Stuart MCA, Hulst R, Engberts JBFN (2006) Langmuir 22:2558–2568
20. Ohnuki H, Saiki T, Kusakari A, Ichihara M, Izumi M (2008) Thin Solid Films 516:8860–8864
21. Huang J, Liu Y, Wang X (2008) J Mol Catal Enzym 55:49–54
22. Sastry M, Kumar A, Mukherjee P (2001) Coll Surf A 181:255–259
23. Benitez JJ, Kopta S, Diez-Perez I, Sanz F, Ogletree DF, Salmeron M (2003) Langmuir 19:762–765
24. Lair D, Alexandre S, Valleton JM (2005) Coll Surf B 45:200–208
25. Stamatatos L, Leventis R, Zuckermann MJ, Silvius JR (1988) Biochemistry 27:3917–3925
26. Rädler JO, Koltover I, Salditt T, Safinya CR (1997) Science 275:810–840
27. Jurkiewicz P, Olzynska A, Langner M, Hof M (2006) Langmuir 22:8741–8749
28. Nishizuka Y (1984) Nature 308:693–698
29. Nishizuka Y (1986) Science 233:305–311
30. Liscovich M, Cantley LC (1994) Cell 77:329–334
31. Siegel DP, Banschbach J, Alford D, Ellens H, Lis LJ, Quinn PJ, Yeagle PL, Bentz J (1989) Biochemistry 28:3703–3709
32. Churchward MA, Rogasevskaia T, Brandman DM, Khosravani H, Nava Atkinson JK, Coorssen JR, 3976 (2008) Biophys J 94:3976–3986

33. Damodaran KV, Merz KM Jr (1993) Langmuir 9:1179–1183
34. Perera L, Essmann U, Berkowitz ML (1996) Langmuir 12:2625–2629
35. Marrink SJ, de Vries AH, Mark AE (2004) J Phys Chem B 108:750–760
36. Siu SWI, Vacha R, Jungwirth P, Bockmann RA (2008) J Chem Phys 128:125103
37. Gauger DR, Selle C, Fritzsche H, Pohle W (2001) J Mol Struct 565–566:25–29
38. Pohle W, Selle C, Fritzsche H, Bohl M (1997) J Mol Struct 408–409:273–277
39. Pohle W, Selle C, Fritzsche H, Binder H (1998) Biospectroscopy 4:267–280
40. Selle C, Pohle W, ibid 281-294
41. Pfeiffer H, Binder H, Klose G, Heremans K (2003) Biochim Biophysica Acta Biomembranes 1609:144–147
42. Pohle W, Selle C (1996) Chem Phys Lipids 82:191–198
43. Pohle W, Selle C, Gauger DR, Brandenburg K (2001) J Biomol Struct Dyn 19:351–364
44. Dunkel R, Hahn M, Borisch K, Neumann B, Ruttinger HH, Tschierske C (1998) Liq Cryst 24:211–213
45. Helmreich B, Hahn M (1999) LaborPraxis 4:64–69
46. Gauger DR, Selle C, Hahn M, Pohle W (2001) Anal Biochem 299:108–110
47. Bour P, Malon P (1995-2009) MCM molecular graphics. Academy of Sciences, Prague
48. Case DA, Darden TA, Cheatham TE III, Simmerling CL, Wang J, Duke RE, Luo R, Merz KM, Pearlman DA, Crowley M, Walker RC, Zhang W, Wang B, Hayik S, Roitberg A, Seabra G, Wong KF, Paesani F, Wu X, Brozell S, Tsui V, Gohlke H, Yang L, Tan C, Mongan J, Hornak V, Cui G, Beroza P, Mathews DH, Schafmeister C, Ross WS, Kollman PA (2006) AMBER 9. University of California, San Francisco
49. Martinez JM, Martinez L (2003) J Comput Chem 24:819–825
50. Snyder RG (1961) J Mol Spectrosc 7:116–144
51. Snyder RG (1979) J Chem Phys 71:3229–3235
52. Jendrasiak GL, Smith RL (2004) Chem Phys Lipids 131:183–195
53. Pand RP, Parsigian VA (1989) Biochim Biophys Acta 988:351–376
54. Katsaras J (1997) Biophys J 73:2924–2929
55. Reck RA, Harwood HJ, Ralston AW (1947) J Org Chem 12:518–522
56. Crossley A, Freeman IP, Hudson BJF, Pierce JH (1959) J Chem Soc 760-764
57. Tristram-Nagle S, Zhang R, Suter RM, Worthington CRM, Sun W-J, Nagle JF (1993) Biophys J 64:1097–1109
58. Jiang ZJ, Wu J, Heberle FA, Mills TT, Klawitter P, Huang G, Costanza G, Feigenson GW (2007) Biochim Biophys Acta 1768:2764–2776
59. Tardieu A, Luzzati V, Reman FC (1973) J Mol Biol 75:711–733
60. Brunauer S (1943) The adsorption of gases and vapors Vol 1. Princeton University Press, Princeton
61. Gauger DR, Binder H, Vogel A, Selle C, Pohle W (2002) J Mol Struct 614:211–220
62. de Oliveira Neto M (1986) J Comput Chem 7:617–628, ibid 629-639
63. Grdadolnik J, Kidric J, Hadzi D (1991) Chem Phys Lipids 59:57–68
64. Selle C, Pohle W, Fritzsche H (1997) Mikrochim Acta Suppl 14:449–450
65. Pearson RH, Pascher I (1979) Nature 281:499–501
66. Hsieh CH, Wu WG (1996) Biophys J 71:3278–3287
67. Mrazkova E, Hobza P, Bohl M, Gauger DR, Pohle W (2005) J Phys Chem B 109:15126–15134
68. Jeffrey GA, Saenger W (1991) Hydrogen bonding in biological structures. Springer, Berlin
69. Jeffrey GA (1969) Acc Chem Res 2:344–352
70. McMullan RK, Mak TCW, Jeffrey GA (1966) J Chem Phys 44:2338–2345
71. Lipscomb LA, Zhou FX, Williams LD (1996) Biopolymers 38:177–181
72. Udachin KA, Ripmeester JA (1999) Nature 397:420–423
73. Zhao W, Moilanen DE, Fenn EE, Fayer D (2008) J Am Chem Soc 30:13927–13937
74. Bruegel W (1957) Einführung in die Ultrarotspektroskopie. Darmstadt, Steinkopff
75. Holy S, Sohar P (1975) Absorption spectra in the infrared region. Akademiai kiado, Budapest
76. Colthup NB, Daly LH, Wiberley SE (1990) Introduction to infrared and Raman spectroscopy. Academic, Boston
77. Günzler H, Heise HM (1996) IR-Spektroskopie. VCH, Weinheim
78. Chalmers JM, Griffiths PR (2002) Handbook of vibrational spectroscopy. Wiley, Chichester
79. Peter K, Vollhardt C (1990) Organische Chemie. VCH Verlagsgesellschaft, Weinheim
80. Pohle W, Gauger DR (2009) J Mol Struct 924–926:144–147
81. Spectral database for organic compounds, SDBS, National institute of AIST, Japan
82. Pouchert CJ (ed) (1985) The Aldrich library of FT-IR spectra. Aldrich, Milwaukee
83. NIST Chemistry WebBook, NIST Standard Reference Database, Gaithersburg
84. Kumar A, Joshi H, Pasricha R, Mandale AB, Sastry M (2003) J Colloid Interface Sci 264:396–401
85. Krueger PJ, Smith DW (1967) Can J Chem 45:1605–1610
86. Hitchcock PB, Mason R, Thomas KM, Shipley GG (1974) Proc Natl Acad Sci USA 71:3036–3040
87. Akutsu H, Ikematsu M, Kyogoku Y (1981) Chem Phys Lipids 28:149–158
88. Boggs J (1987) Biochim Biophys Acta 906:353–404
89. Shin TB, Leventis R, Silvius JR (1991) Biochemistry 30:7491–7497
90. Lewis RNAH, McElhaney RN (1993) Biophys J 64:1081–1096
91. Pohle W, Selle C, Gauger DR, Zantl R, Artzner F, Rädler JO (2000) Phys Chem Chem Phys 2:4642–4650
92. Sandermann H Jr (1976) Eur J Biochem/FEBS 62:479–484
93. Marsh D (1997) Biophys J 72:2834–2836
94. Schorn K, Marsh D (1996) Biochemistry 35:3831–3836
95. Dawson RMC, Irvine RF, Bray J, Quinn PJ (1984) Biochem Biophys Res Commun 125:836–842
96. Huang P, Perez J, Loew G (1994) J Biomol Struct Dyn 11:927–956
97. Thieleman DP, Berendsen HJC (1996) J Chem Phys 105:4871–4880
98. Binder H, Pohle W (2000) J Phys Chem B 104:12039–12048
99. Binder H, Kohlstrunk B, Pohle W, ibid:12049–12055